

Chemical, electrical, and structural properties of Ni/Au contacts on chemical vapor cleaned *p*-type GaN

Cite as: Journal of Applied Physics **91**, 9151 (2002); <https://doi.org/10.1063/1.1471578>

Submitted: 16 October 2001 • Accepted: 01 March 2002 • Published Online: 20 May 2002

P. J. Hartlieb, A. Roskowski, R. F. Davis, et al.



View Online



Export Citation

ARTICLES YOU MAY BE INTERESTED IN

[Effects of surface treatments and metal work functions on electrical properties at p-GaN/metal interfaces](#)

Journal of Applied Physics **81**, 1315 (1997); <https://doi.org/10.1063/1.363912>

[Low-resistance ohmic contacts to p-type GaN achieved by the oxidation of Ni/Au films](#)

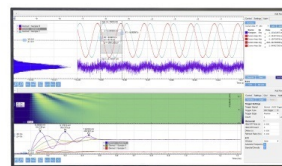
Journal of Applied Physics **86**, 4491 (1999); <https://doi.org/10.1063/1.371392>

[p-GaN surface treatments for metal contacts](#)

Applied Physics Letters **76**, 415 (2000); <https://doi.org/10.1063/1.125772>

Challenge us.

What are your needs for periodic signal detection?



Zurich
Instruments



Chemical, electrical, and structural properties of Ni/Au contacts on chemical vapor cleaned *p*-type GaN

P. J. Hartlieb, A. Roskowski, and R. F. Davis^{a)}

Department of Materials Science and Engineering, North Carolina State University, Raleigh, North Carolina 27695-7907

R. J. Nemanich

Department of Physics, North Carolina State University, Raleigh, North Carolina 27695-8202

(Received 16 October 2001; accepted for publication 1 March 2002)

Chemical vapor cleaned, Mg-doped, *p*-type GaN(0001) surfaces and Ni/Au contacts deposited on these surfaces have been studied using several characterization techniques. Stoichiometric surfaces without detectable carbon and an 87% reduction in the surface oxygen to 2 ± 1 at. % were achieved. The binding energies of the Ga 3*d* and N 1*s* core level photoelectron peaks were reduced by 0.5 ± 0.1 eV following the chemical vapor clean. The band bending at the clean surface was measured to be 0.8 ± 0.1 eV. As-deposited Ni/Au contacts on chemical vapor cleaned surfaces exhibited significantly less rectification in the low voltage region (< 2 V) compared to identical contact structures on conventional HCl treated surfaces. The specific contact resistance of these contacts deposited on chemical vapor cleaned surfaces and subsequently annealed at 450 °C for 30 seconds was $3 \pm 2 \Omega \text{ cm}^2$. Improved ohmic behavior and a specific contact resistance of $4 \pm 2 \Omega \text{ cm}^2$ was obtained for contacts deposited on HCl treated surfaces and annealed using the same schedule. The formation of Au:Ga and Au:Ni solid solutions was observed for contacts on HCl treated surfaces following the 450 °C anneal. There were significantly less interfacial reactions for annealed contacts on chemical vapor cleaned surfaces. The values of specific contact resistance, sheet resistance, and transfer length of the annealed contacts deposited on both chemical vapor cleaned and HCl treated surfaces and measured from room temperature to 140 °C did not change during three successive thermal cycles within this range. © 2002 American Institute of Physics.
[DOI: 10.1063/1.1471578]

I. INTRODUCTION

The achievement of *p*-type GaN has allowed the development of blue and green light emitting diodes (LEDs), blue emitting laser diodes, as well as nitride based heterojunction bipolar transistors and field effect devices.^{1–5} The future improvement of these devices rests in part on a detailed understanding of the metal/*p*-GaN interface and the development of approaches to reduce the specific contact resistance, which has been consistently reported^{6–25} between 1×10^{-4} and $1 \Omega \text{ cm}^2$. The large specific contact resistance proceeds directly from the inherent difficulties involved in acceptor doping with Mg, which is the most common method for achieving *p*-type conducting GaN. The current limitations in the quantity of Mg that can be incorporated during growth ($\sim 1 \times 10^{20} \text{ cm}^{-3}$)^{26–28} as well as the large acceptor ionization energy (~ 300 meV)²⁹ limits the percentage of the atomic concentration that is ionized at room temperature to within the reported^{25,26} range of 0.1%–2.0%. Both limitations make it difficult to fabricate a tunneling ohmic contact to *p*-GaN in a manner similar to that used in other metal–semiconductor systems.³⁰ The large ~ 6.5 eV work function of *p*-GaN and the absence of any metal with a work function greater than 5.8 eV make it impossible to select a contact metal based on matching the work functions of the materials. Additionally,

there is a tenacious layer of native contamination on the as-grown surface that is ~ 2 nm thick, which can add an additional 0.2 eV to the barrier height.^{31,32} The nature of the native surface contamination has been discussed in a previous study.³³ In light of the aforementioned challenges, the Ni-based contact schemes previously employed in making ohmic contacts to GaAs (Refs. 34 and 35) have been applied to *p*-GaN films, due in part to their ability to penetrate the native oxide during annealing. The Ni/Au contact scheme in particular has achieved widespread use in both commercially produced LEDs as well as other GaN-based devices that contain a *p*-type GaN epilayer.^{3,5}

Although Ni has been shown to partially disperse the native contamination at the *p*-type GaN surface,³² research concerned with multiple *in situ* and *ex situ* surface preparation methods has been conducted in an attempt to remove contaminants,^{14,15,17–19,21,31,32,37–39} and/or modify the surface electronic properties,^{17,32,38,39} and/or improve the epitaxial quality of the metallization.³⁶ A dilute HCl bath, which is the most common *ex situ* cleaning technique,^{6–10,14,15,37} has been shown to only slightly reduce O and C contamination at the surface.³¹ Analyses of the results of similar *ex situ* treatments that used room temperature aqua-regia (HCl:HNO₃ 1:1),^{12–14} boiling aqua-regia,^{14–16,18–20} boiling KOH,²¹ BOE,^{22–24,32} dilute HF,²⁵ or a sequential dip in multiple chemical baths^{19,24,37} have also revealed limited success in cleaning and/or modifying the properties of the *p*-type GaN surface.

^{a)}Electronic mail: robert_davis@ncsu.edu

These results are expected given the finite period between pulling the samples from solution and loading them into ultrahigh vacuum (UHV). The rapid reformation of the contamination layer has been confirmed in a study that investigated the effects of Ar ion sputtering on the surface properties of *p*-type GaN.³² Additional *in situ* methods of surface preparation, including UHV annealing^{37,38} and plasma techniques,^{6,40} have been either ineffective at removing native contamination or damaging to the semiconductor surface.

Numerous studies^{6–9,11–13,16,23,41–44} have investigated the effects of annealing Au/Ni/*p*-GaN contact structures between 300 and 850 °C in a N₂ ambient from 30 s to 10 min in an attempt to overcome the deficiencies of *in situ* and *ex situ* surface preparation. The dispersal of the native contamination^{32,41} and/or the formation of reaction products either within the contact metallization or at the metal–semiconductor interface^{8,9,12,13,16,43} have been proposed as possible mechanisms for the reduction of the specific contact resistance. As the dispersal of native contamination is accompanied by additional reactions within the contact structure,⁴¹ the effects of contamination removal alone on the ohmic behavior have not been assessed. Although most studies report a decrease in the specific contact resistance following a postmetallization anneal at temperatures between 500 and 600 °C, there is still considerable disagreement regarding the temperature at which specific interfacial reactions occur, the products of those reactions, and the mechanism through which newly formed phases subsequently reduce the specific contact resistance.

Studies of other metal–semiconductor systems have also shown⁴⁵ that there is some correlation between the grain size and the orientation of the grains of the as-deposited metal and the quantity of contamination on the semiconductor surface prior to metallization. More importantly, marked differences in the thermal stability of the interface have been observed for contacts on atomically clean and contaminated semiconductor surfaces.⁴⁵ This has been clearly shown in the Au/GaAs system wherein following a postmetallization anneal, contacts on contaminated surfaces formed nonuniform protrusions at the metal–semiconductor interface.⁴⁵ By contrast, the interface for contacts on atomically clean GaAs surfaces remained atomically flat and abrupt. Liu *et al.*³⁶ have suggested that the correlation between surface cleanliness and the degree of epitaxy and/or crystallinity is equally applicable to the metal/GaN systems. Rutherford backscattering measurements were used to study the effects of *ex situ* chemical pretreatments on the channeling yields of Pd(111) aligned backscattering spectra from Pd/GaN structures. The variation in the channeling yield following *ex situ* cleaning in boiling aqua regia, HCl:H₂O, or HF:H₂O is attributed to previously observed differences in the quantity of native contamination removed by each *ex situ* pretreatment. However, the amount of contamination on the surfaces used in the study above as well as the effects that this contamination may have on the reaction products following postmetallization annealing has not been described.

The present work is a comprehensive study of the chemical, structural, and electrical properties of Ni/Au con-

tacts deposited on the surfaces of *p*-type GaN films, which have been pretreated using an NH₃-based, high-temperature chemical vapor clean (CVC). The effectiveness of the CVC process at removing native surface contamination as well as the influence of surface contamination on the electrical and structural properties of the contact structures have been studied using various types of characterization techniques.

II. EXPERIMENT

Each 1 μm thick, Mg doped, Ga terminated^{14,46} GaN(0001) film used in this study was grown at 1020 °C via organometallic vapor phase epitaxy (OMVPE) on a 100 nm thick AlN buffer layer previously deposited at 1100 °C on an on axis 6H-SiC(0001) substrate. The films were subsequently annealed under flowing N₂ at 800±10 °C for 30 s in an AG-Associates 610 rapid thermal annealing unit to break the Mg–H bonds⁴⁷ and thus activate the Mg dopant.

Capacitance voltage (*C–V*) measurements on the doped films were obtained at a frequency of 10 kHz using a Hewlett Packard 4284A *C–V* measurement system and a MDC mercury probe station. Hall effect measurements were conducted on a separately diced section of the same wafer using a Keithley 617 programmable electrometer and Keithley 220 programmable current source. The activation anneals for the latter sections were performed in a N₂ ambient at 800 °C for 45 s using a custom-made rapid thermal annealing unit.

Tungsten was sputtered onto the backside of the SiC substrates to assist in radiative heating of the transparent samples throughout the *in situ* preparation process. Prior to loading, the films were sequentially cleaned in trichloroethylene (TCE), acetone, and methanol baths for 1 min each followed by a 10 min dip in 49% hydrochloric acid and a 10 s rinse in deionized (DI) water. The details of the effects of this cleaning process have been published elsewhere.³¹ Films that were not subjected to the *in situ* processing procedures described below and in succeeding sections are termed “as-loaded.” The samples were fastened to a molybdenum plate and subsequently attached to a molybdenum sample holder, which facilitated the transfer process throughout the experiment. Approximately 15 min elapsed between pulling the sample from the DI rinse and loading it into an integrated surface analysis and growth system operating at a base pressure of (4×10^{−10}–3×10^{−9}) Torr. The system was equipped with x-ray and ultraviolet photoelectron spectroscopy units, as well as electron beam metallization and chemical vapor cleaning facilities.

An ammonia-based high-temperature chemical vapor clean³¹ was used to obtain a clean, ordered *p*-type GaN surface. To achieve these surfaces, the sample was initially heated to 500±10 °C, whereupon the ammonia was introduced. The sample was then heated to 830±20 °C and held for 15 min at a process pressure of (9±1)×10^{−5} Torr. As the distance between the ammonia doser and the sample was ~5 cm, the partial pressure of ammonia at the sample surface may have been as much as an order of magnitude greater than the system pressure. Upon cooling to 200±10 °C the sample was immediately transferred in UHV to the requisite chambers for x-ray photoelectron spectroscopy

(XPS) and ultraviolet photoelectron spectroscopy (UPS) investigations and subsequent metallization. The surface temperature was monitored throughout the process with an Ircon infrared pyrometer having an emissivity (ϵ) setting of 0.5. Temperatures outside the operating range of the pyrometer ($<600^\circ\text{C}$) were measured using the thermocouple mounted immediately behind the sample.

XPS measurements were conducted using a Fisons XR3 dual anode x-ray source coupled to a Fisons CLAM II hemispherical electron energy analyzer with a mean radius of 100 mm operating at a base pressure of $(1 \pm 1) \times 10^{-9}$ Torr. The resolution of the analyzer was 1.0 eV although the absolute peak positions could be measured to within 0.1 eV. All core level spectra were fit using linear background subtraction and a mixed Gaussian–Lorentzian peak type. UPS measurements were made using an Omicron HIS13 gas discharge lamp together with a hemispherical electron energy analyzer whose mean radius was 50 mm. A negative bias of 4 V was applied to the sample throughout each measurement to overcome the work function of the spectrometer. The resolution of the analyzer was approximately 0.1 eV. All spectra were acquired at an operating pressure of $(7 \pm 3) \times 10^{-9}$ Torr while the base pressure of the system was $<3 \times 10^{-10}$ Torr (the increased pressure is due to the He from the discharge lamp). The Fermi level position was determined from UPS measurements made on clean 50 nm thick Ni films. All metal depositions were conducted using an electron beam evaporation system equipped with a quartz crystal thickness monitor operating at a base pressure of $(2 \pm 1) \times 10^{-10}$ Torr. The contact structures consisted of a 50 nm Ni overlayer deposited on either CVC or as-loaded *p*-type GaN surfaces followed by a 100 nm Au cap.

Samples were patterned using standard photolithographic techniques and subsequently etched in 1:1:1 $\text{HNO}_3:\text{HCl}:\text{DI}$ solution to reveal transfer length method (TLM)⁴⁸ test structures with $300 \times 1500 \mu\text{m}^2$ rectangular pads spaced at distances between 5 and 30 μm . Contact structures were subsequently annealed under flowing N_2 at 450°C for 30 s in an AG Associates 610 rapid thermal annealing unit. A 4 in. Si wafer with a bonded *K*-type thermocouple was loaded directly into the oven to provide an independent measurement of the process temperature. The specific contact resistance (ρ_c), sheet resistance (ρ_s), and transfer length (L_T) were calculated from the slope and intercepts obtained from a linear regression of the resistance measured at a fixed current level of 1.5×10^{-6} A as a function of contact spacing [i.e., $R(l)$ versus l]. Current–voltage (I – V) measurements were conducted using a Keithley 236 source measure unit and probe station equipped with a heated stage for temperature dependent measurements. Contact structures were measured using tungsten probe tips with a 7 μm radius and a taper of 0.200–0.220 in. During electrical measurements the annealed contact structures were subjected to repeated thermal cycling to 140°C to examine changes in the electrical properties at elevated temperatures. The sample temperature was measured by a handheld *K*-type thermocouple in touching contact with the *p*-type GaN surface. During each thermal cycle the sample was heated from room temperature to 140°C whereupon I – V measurements

were made on a single TLM test structure. The time required to make electrical measurements at this temperature was approximately 40 min. Immediately following the high-temperature measurements each sample was cooled to room temperature and the I – V measurements were repeated. This entire process was repeated a total of three times for contact structures on both CVC and as-loaded surfaces.

Atomic force microscopy (AFM) images were acquired in the contact mode using a Park Scientific Instruments auto probe M5 having a Si tip. X-ray diffraction measurements were performed on a Phillips X-pert system using $\text{Cu } K\alpha$ ($\lambda = 0.1542$ nm) radiation.

III. RESULTS

A. Chemical vapor cleaning (CVC) of the GaN(0001) surface

The spectrum of the as-loaded *p*-GaN film shown in Fig. 1 indicates that the C 1s core level located at 285.0 ± 0.1 eV [full width at half maximum (FWHM) = 1.8 eV] lies within the 284.8–285.3 eV range reported in the literature for adventitious carbon.^{31,49,50} Therefore charging effects and subsequent shifts in the photoelectron peak positions were considered to be negligible. A C concentration of ~ 6 at. % was calculated for the as-loaded surface using the integrated intensity and the C 1s sensitivity factor of 0.25. Following the CVC process, the C signal was reduced below the ~ 0.3 at. % limit of detection of the XPS.⁵⁰

The O 1s core level spectra from the as-loaded surface, presented in Fig. 1, was fit with a single broad peak located at 532.4 ± 0.1 eV (FWHM = 2.4 eV). Following the CVC process there was a significant reduction in the peak intensity and a shift to lower binding energy as evidenced by the final peak location at 531.1 ± 0.1 eV (FWHM = 1.7 eV). The O concentrations on the as-loaded and CVC treated surfaces, calculated using the integrated intensities and the corresponding O 1s sensitivity factor of 0.660 were ~ 14 and 2 ± 1 at. %, respectively.

Figure 2(a) shows the Ga 3d spectra obtained from the as-loaded and CVC treated surfaces, which were fit with single peaks located at 19.6 ± 0.1 eV (FWHM = 1.8 eV) and 19.0 ± 0.1 eV (FWHM = 2.0 eV), respectively. An equivalent shift was observed for the N 1s core level in Fig. 2(b), whose peak locations on the as-loaded and CVC treated surfaces were 397.1 ± 0.1 eV (FWHM = 1.5 eV) and 396.6 ± 0.1 eV (FWHM = 1.8 eV), respectively. The magnitude and direction of the shifts were in excellent agreement with the shift observed for the core level feature identified in the valence band spectra acquired via UPS and shown in Fig. 3. The Ga:N ratios, determined from the integrated intensities of the Ga 3d and N 1s core levels and corresponding sensitivity factors (Ga 3d, 0.310 and N 1s, 0.420), were calculated to be 1.1 and 0.9 for the as-loaded and CVC treated surfaces, respectively. The location of each core level photoelectron peak on the as-loaded and CVC treated surfaces as well as the corresponding shifts are shown in Table I.

The UPS spectra also indicate that the Fermi level is pinned well above the valence band maximum (VBM) on the as-loaded surface. The exact position of the VBM on this

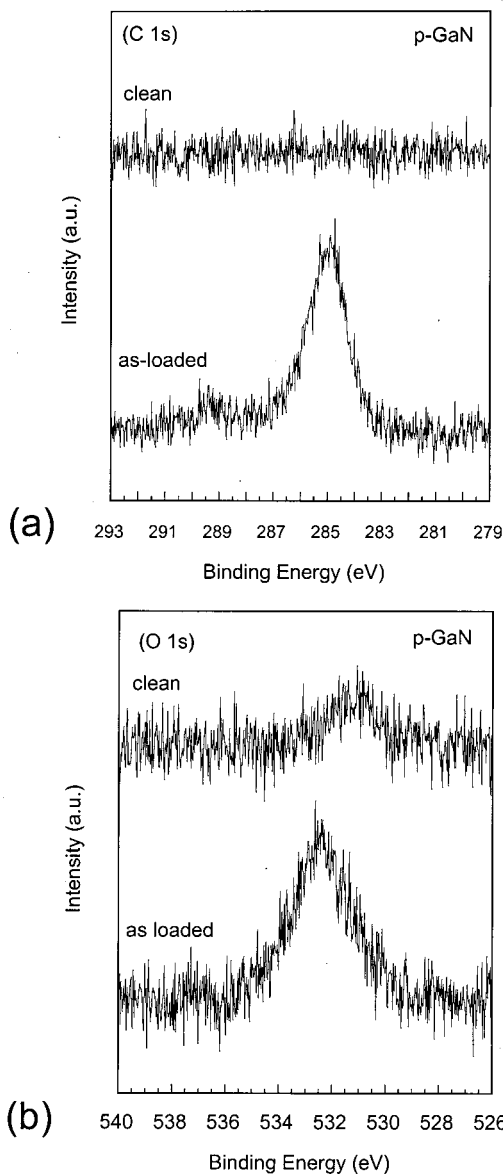


FIG. 1. XPS results showing (a) C $1s$ and (b) O $1s$ core level photoelectron peaks from the as-loaded and chemical vapor cleaned (CVC) p -GaN surfaces. The C $1s$ and O $1s$ spectra were acquired using Al $K\alpha$ ($h\nu = 1486.6$ eV) and Mg $K\alpha$ ($h\nu = 1253.6$ eV) radiation, respectively.

surface is difficult to determine due to the exponential nature of the turn-on for the contaminated surface. Following the CVC process, there is a significant shift in the VBM to a lower binding energy. The VBM on the clean surface, located by taking a linear fit of the high kinetic energy side of the spectrum shown in the inset of Fig. 3, was 1.1 ± 0.1 eV below the Fermi level. Assuming that the Mg acceptor level lies ~ 300 meV above the VBM and a room temperature band gap of 3.4 eV,²⁹ the subsequent downward band bending and electron affinity were calculated to be 0.8 ± 0.1 and 2.6 ± 0.1 eV, respectively. The apparent disagreement with previously measured values of the electron affinity³³ will be discussed in a later section.

B. Electrical measurements

Calculations from the results of capacitance–voltage measurements of the annealed p -GaN film used in this re-

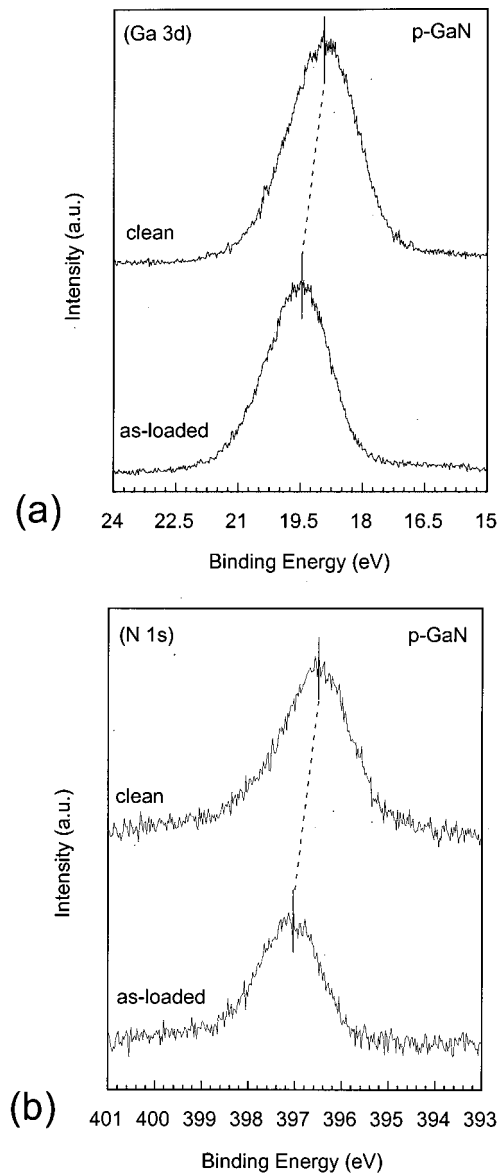


FIG. 2. XPS results showing (a) Ga $3d$ and (b) N $1s$ core level photoelectron peaks from the as-loaded and the CVC p -GaN surfaces. The Ga $3d$ and the N $1s$ spectra were acquired using Mg $K\alpha$ ($h\nu = 1253.6$ eV) radiation. The dashed lines are visual aids that indicate the shifts in energy.

search indicated a net ionized impurity concentration ($N_A - N_D$) of $\sim 1 \times 10^{18}$ cm⁻³. Hall effect measurements revealed a carrier concentration, mobility, and resistivity of 1.1×10^{17} cm⁻³, 0.8 cm²/V s, and 81.6 (Ω cm) ($\rho_{\text{sheet}} = 8.16 \times 10^5$ Ω /sq), respectively. The marked difference between the net ionized impurity and carrier concentrations is attributed to the differences in characteristics of the measurement techniques. The reverse bias applied to the Schottky contact during a $C-V$ measurement and the subsequent increase in downward band bending allows for full ionization in the depletion region.⁵¹ Kozodoy *et al.*⁵¹ have suggested that in the low frequency regime (~ 10 kHz) each Mg acceptor has an adequate period of time to change its ionization state and contribute to the capacitance. However, the Hall technique only measures free carriers generated by the partially ionized

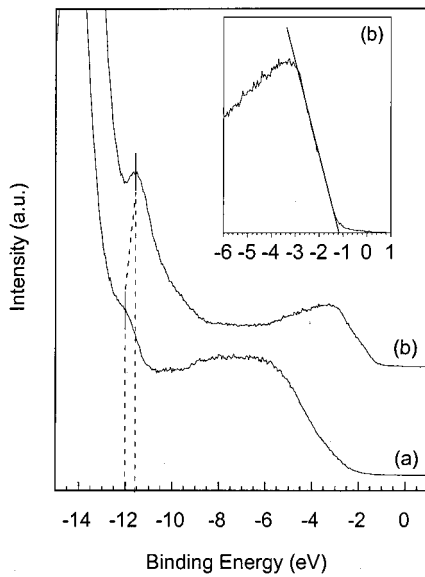


FIG. 3. UPS valence band spectra from the (a) as-loaded and (b) CVC *p*-GaN surfaces. The dashed lines indicate the shift of the bulk N feature. A linear fit of the high kinetic energy side of spectra (b) and the subsequent position of the valence band maximum (VBM) on the clean surface are shown in the inset. All spectra were acquired using the He I photon line ($h\nu=21.2$ eV). The binding energy is measured with respect to the Fermi level ($E_F=0$ eV).

acceptors in the bulk. As noted above, the carrier contribution from the acceptors in the bulk is limited by the ~ 300 meV ionization energy of the Mg acceptor.

The $I-V$ characteristics for the as-deposited Ni/Au contacts on both the as-loaded and the CVC *p*-type GaN surfaces are shown in Fig. 4. Values of ρ_c , ρ_s , and L_T for the as-deposited contact structures on a CVC surface were calculated to be $2 \pm 2 \Omega \text{ cm}^2$, $(3.7 \pm 0.5) \times 10^6 \Omega/\text{sq}$, and $8 \pm 2 \mu\text{m}$, respectively. The origin of the large uncertainty in the specific contact resistance will be discussed in a later section. Values of ρ_c , ρ_s , and L_T for the as-deposited contact structures on the as-loaded *p*-type GaN surface could not be calculated because the total resistance did not monotonically increase with contact spacing. In the low voltage region (i.e., <2 V) contacts on the CVC surface show less rectification than those on the as-loaded surface, which is consistent with the removal of native surface contamination and a reduction in the Schottky barrier height. In the high voltage region (i.e., >5 V) contacts on the as-loaded surface passed

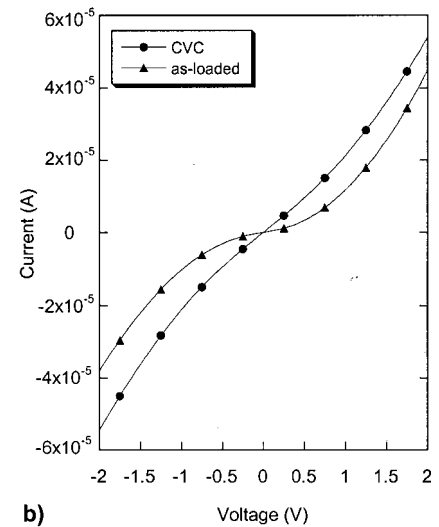
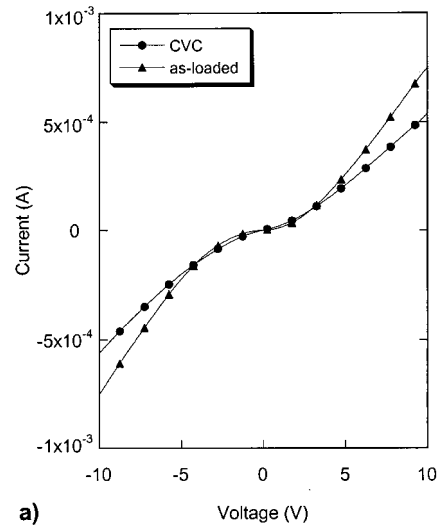


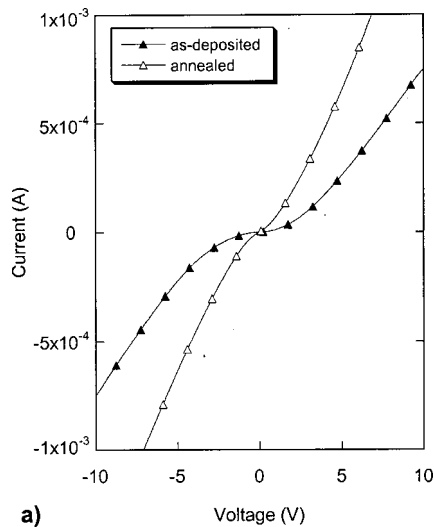
FIG. 4. Current–voltage ($I-V$) plots for as-deposited Ni/Au contacts on as-loaded (triangle) and CVC (circle) *p*-type GaN surfaces. The low voltage region has been magnified in (b). The contact spacing was $5 \mu\text{m}$.

greater current at equivalent voltages than those on a CVC surface. Most prior studies of the effects of native surface contamination have employed postmetallization annealing which obscures the interface properties.

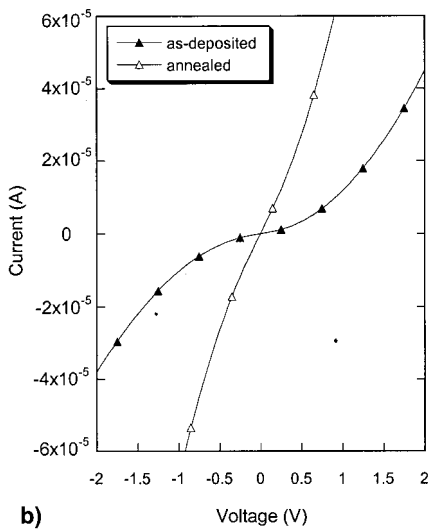
The $I-V$ characteristics of the as-deposited and annealed Ni/Au contacts deposited on as-loaded and CVC surfaces are

TABLE I. XPS core level photoelectron peak positions and full width at half maxima (FWHM) from as-loaded and chemical vapor cleaned (CVC) *p*-type GaN surfaces. The Ga 3*d*, N 1*s*, and O 1*s* spectra were acquired using Mg *Kα* ($h\nu=1253.6$ eV) radiation. The C 1*s* spectrum was acquired using Al *Kα* ($h\nu=1486.6$ eV) radiation. The error in both the peak position and full width at half maximum is ± 0.1 eV.

Peak	As-loaded ± 0.1		Clean ± 0.1		Shift (eV)
	Position (eV)	FWHM (eV)	Position (eV)	FWHM (eV)	
O 1 <i>s</i>	532.4	2.4	531.1	1.7	1.3
C 1 <i>s</i>	285	1.8	NA	NA	NA
Ga 2 <i>p</i>	1118	1.8	1117.5	2	0.5
Ga 3 <i>d</i>	19.6	1.8	19	2	0.6
N 1 <i>s</i>	397.1	1.5	396.6	1.8	0.5

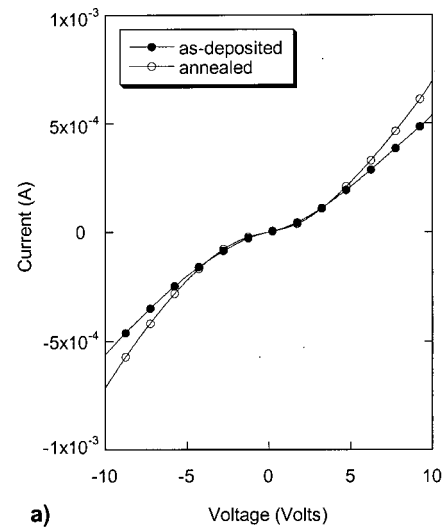


a)

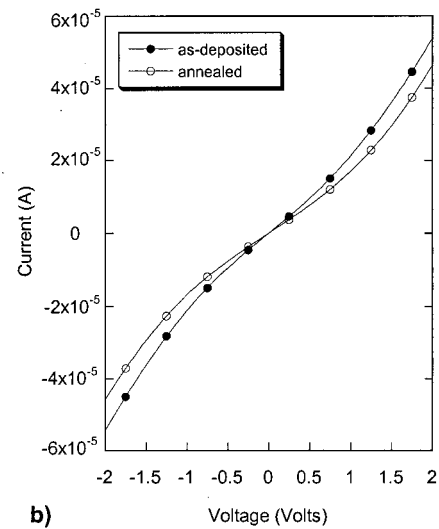


b)

FIG. 5. Current–voltage (I – V) plots of the as-deposited (closed triangles) and annealed 450 °C (open triangles) for Ni/Au contacts on as-loaded p -type GaN surfaces. The low voltage region has been magnified in (b). The contact spacing was 5 μm .



a)



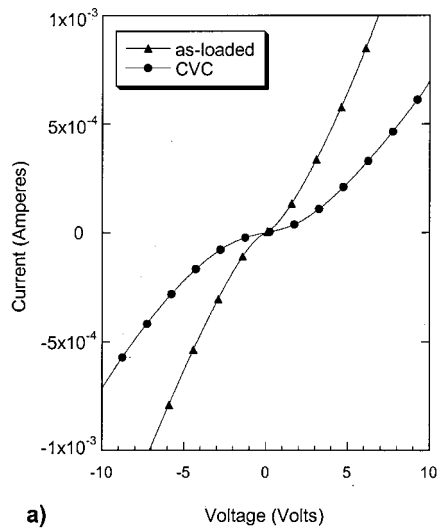
b)

FIG. 6. Current–voltage (I – V) plots of the as-deposited (closed circles) and annealed 450 °C (open circles) Ni/Au contacts on CVC p -type GaN surfaces. The low voltage region has been magnified in (b). The contact spacing was 5 μm .

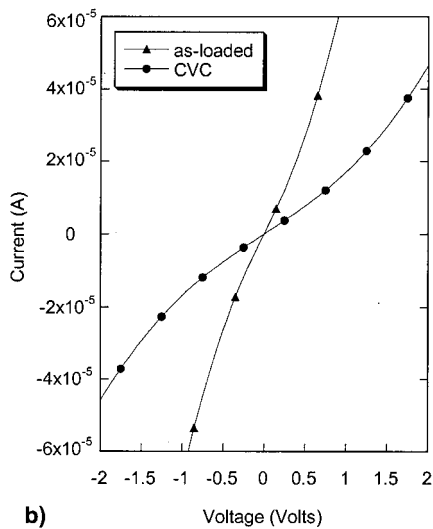
compared in Figs. 5 and 6, respectively. The data presented in Fig. 5 show a significant improvement in the ohmic properties and a marked increase in the current passed at all voltages for the contacts on the as-loaded surfaces following annealing at 450 °C. Calculated values of ρ_c , ρ_s , and L_T for the annealed contact structures were $4 \pm 2 \Omega \text{ cm}^2$, $(6.7 \pm 0.7) \times 10^5 \Omega/\text{sq}$, and $23 \pm 4 \mu\text{m}$, respectively. Within the calculated experimental error there was no change in ρ_c , ρ_s , or L_T for the contacts on the CVC surface after annealing at 450 °C, as shown in Fig. 6.

Figures 8(a) and 8(b) show a portion of the I – V data acquired during heating and after repeated thermal cycling of contacts on the as-loaded and the CVC surfaces, respectively. Comprehensive numerical results for contacts on as-loaded and CVC surfaces are presented in Tables II and III, respectively. Values of ρ_c , ρ_s , and L_T for contact structures on CVC surfaces heated to 140 °C during the first thermal cycle were calculated to be $0.5 \pm 0.3 \Omega \text{ cm}^2$, (4.4 ± 0.5)

$\times 10^5 \Omega/\text{sq}$, and $10 \pm 2 \mu\text{m}$, respectively. The contacts performed consistently through three successive thermal cycles without degradation, as shown by the absence of any change in the room temperature and elevated temperature values for ρ_c , ρ_s , and L_T . Although contact structures on as-loaded surfaces showed some degradation with repeated thermal cycling, as shown in Fig. 8, the uncertainty in the calculated values for ρ_c , ρ_s , and L_T are sufficiently large that these effects cannot be quantified. Values of ρ_c , ρ_s , and L_T for contact structures on the as-loaded surfaces heated to 140 °C during the first thermal cycle were determined to be $0.5 \pm 0.1 \Omega \text{ cm}^2$, $(8.8 \pm 0.5) \times 10^4 \Omega/\text{sq}$, and $24 \pm 2 \mu\text{m}$, respectively. The differences in the values of ρ_s between individual contact structures on as-loaded and CVC surfaces may be attributed to nonuniformities in the Mg doping level over the p -type GaN surface. These nonuniformities are indirectly evidenced by the large FWHM of the Ga 3d and N 1s photoelectron peaks and are discussed in the following sections.



a)



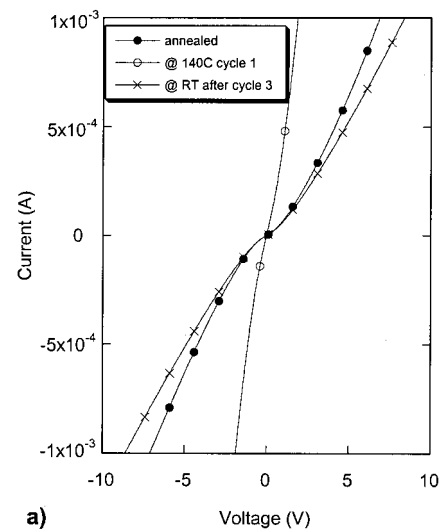
b)

FIG. 7. Current–voltage (I – V) plots of the annealed ($450\text{ }^\circ\text{C}$) Ni/Au contacts on as-loaded (triangles) and CVC (circles) p -type GaN surfaces. The low voltage region has been magnified in (b). The contact spacing was $5\text{ }\mu\text{m}$.

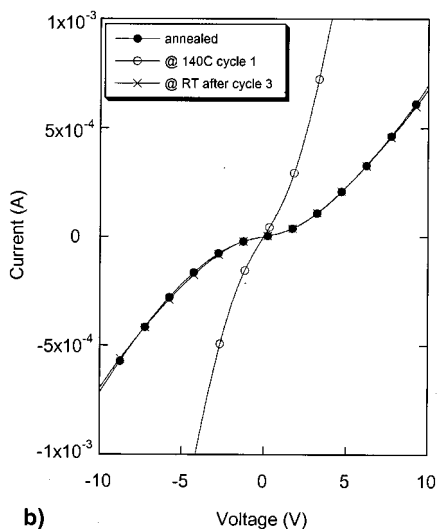
C. Structure and morphology

Atomic force microscopy measurements on contact structures deposited on both as-loaded and CVC surfaces following all thermal processing steps revealed rms roughness values of 8.5 ± 2.0 and 8.0 ± 1.5 nm, respectively. Measurements made on a section of untreated p -type GaN from the same parent wafer without any contact metallization resulted in an rms roughness value of 8.0 ± 1.5 nm. This indicates that the roughness of the parent wafer is sufficiently large that any effects due to either the surface treatment or the postmetallization annealing cannot be observed.

Figure 9 shows XRD ω – 2θ scans for Ni/Au contacts on as-loaded p -type GaN surfaces following all thermal processing. Peaks 1, 2, and 3 are attributed to GaN, SiC, and AlN reflections, respectively. Peak 4, which is attributed to Au (111), is consistent with epitaxial growth of the Au capping layer on the Ni (111) plane. The location of peak 5 is close to that for the predicted values of the (111) reflections from



a)



b)

FIG. 8. (a) Temperature dependent current–voltage (I – V) plots for Ni/Au contacts on as-loaded p -type GaN surfaces at room temperature (closed circles), $T=140\text{ }^\circ\text{C}$ (open circles), and room temperature following all three cycles to $140\text{ }^\circ\text{C}$ (crosses). The contact spacing was $5\text{ }\mu\text{m}$. (b) Temperature dependent current–voltage (I – V) plots for Ni/Au contacts on CVC p -type GaN surfaces at room temperature (closed circles), $T=140\text{ }^\circ\text{C}$ (open circles), and room temperature following all three cycles to $140\text{ }^\circ\text{C}$ (crosses). The contact spacing was $5\text{ }\mu\text{m}$.

Au:Ga (90:10) and Au:Ni (90:10) solid solutions. It is proposed that these new phases are formed during the postmetallization anneal. The absence of the Ni (111) reflection will be discussed in later sections. At this point the origin of the reflection observed at $2\theta \sim 50^\circ$ is unknown and requires further study. However, a similar feature identified in ω – 2θ scans of annealed Au/Pd/ p -GaN contact structures suggests that this reflection is associated with an additional Au–Ga phase.

Figure 10 shows XRD ω – 2θ scans for Ni/Au contacts on CVC p -type GaN surfaces following all thermal processing. Peaks 1, 2, 3, and 4 correspond to the same GaN, SiC, AlN, and Au reflections, respectively, described above. Peak 5, which has been attributed to Ni (111), is consistent with other studies of FCC metals on GaN (Ref. 36) wherein the

TABLE II. Temperature dependence of the specific contact resistance (ρ_c), sheet resistance (ρ_s), and transfer length (L_T) for Ni/Au contacts on as-loaded *p*-type GaN surfaces. The contact set was repeatedly heated to 140 °C and cooled to room temperature for a total of three thermal cycles. Current–voltage measurements were conducted at both room temperature and 140 °C for each cycle. The specific contact resistance (ρ_c) and sheet resistance (ρ_s) were calculated using the transfer length method (TLM).

	State	ρ_c (Ω cm ²)	ρ_s (Ω /sq)	L_T (μ m)
	As-deposited	NR	NR	NR
	Annealed	4 ± 2	(6.7 ± 0.7) × 10 ⁵	23 ± 4
1.	$T = 140$ °C	0.5 ± 0.1	(8.8 ± 0.5) × 10 ⁴	24 ± 2
	$T = RT$	4 ± 1	(7.3 ± 0.6) × 10 ⁵	24 ± 3
2.	$T = 140$ °C	0.6 ± 0.2	(7.7 ± 0.7) × 10 ⁴	28 ± 3
	$T = RT$	4 ± 1	(7.0 ± 0.5) × 10 ⁵	23 ± 2
3.	$T = 140$ °C	0.5 ± 0.3	(9 ± 1) × 10 ⁴	23 ± 4
	$T = RT$	3.6 ± 0.9	(7.1 ± 0.5) × 10 ⁵	23 ± 2

(111) plane of the metal is crystallographically matched to the (0001) oriented *p*-GaN substrate. The shoulder on the Au (111) reflection will be discussed in later sections. The tabulated values in the insets of Figs. 9 and 10 compare the expected and measured values for each reflection.

IV. DISCUSSION

The full width at half maxima of the Ga 3*d* (FWHM = 2.0 eV) and N 1*s* (FWHM = 1.8 eV) photoelectron peaks measured on the CVC surface are significantly larger than the 1.2–1.5 eV values previously observed by the present authors. This increase may be attributed to the variation in the position of the valence band maximum (VBM) over the sample surface and is evidenced by the relatively gradual turn-on observed in the valence band spectra compared to that for other *p*-type GaN films grown in the same reactor.³³ The variation in the position of the VBM effectively increases the width of the spectrum and subsequently decreases the calculated value for the electron affinity (χ).

The uncertainty in the position of the VBM will lead to differences in the Schottky barrier height following Ni depo-

TABLE III. Temperature dependence of the specific contact resistance (ρ_c), sheet resistance (ρ_s), and transfer length (L_T) for Ni/Au contacts on chemical vapor cleaned (CVC) *p*-type GaN surfaces. The contact set was repeatedly heated to 140 °C and cooled to room temperature for a total of three thermal cycles. Current–voltage measurements were conducted at both room temperature and 140 °C for each cycle. The specific contact resistance (ρ_c) and sheet resistance (ρ_s) were calculated using the transfer length method (TLM).

	State	ρ_c (Ω cm ²)	ρ_s (Ω /sq)	L_T (μ m)
	As-deposited	2 ± 2	(3.7 ± 0.5) × 10 ⁶	8 ± 2
	Annealed	3 ± 2	(4.1 ± 0.5) × 10 ⁶	9 ± 2
1.	$T = 140$ °C	0.5 ± 0.3	(4.4 ± 0.5) × 10 ⁵	10 ± 2
	$T = RT$	3 ± 2	(4.6 ± 0.5) × 10 ⁶	8 ± 2
2.	$T = 140$ °C	0.5 ± 0.3	(4.4 ± 0.5) × 10 ⁵	10 ± 2
	$T = RT$	4 ± 3	(4.2 ± 0.7) × 10 ⁶	10 ± 3
3.	$T = 140$ °C	0.5 ± 0.2	(4.4 ± 0.5) × 10 ⁵	10 ± 2
	$T = RT$	4 ± 3	(4.4 ± 0.8) × 10 ⁶	10 ± 3

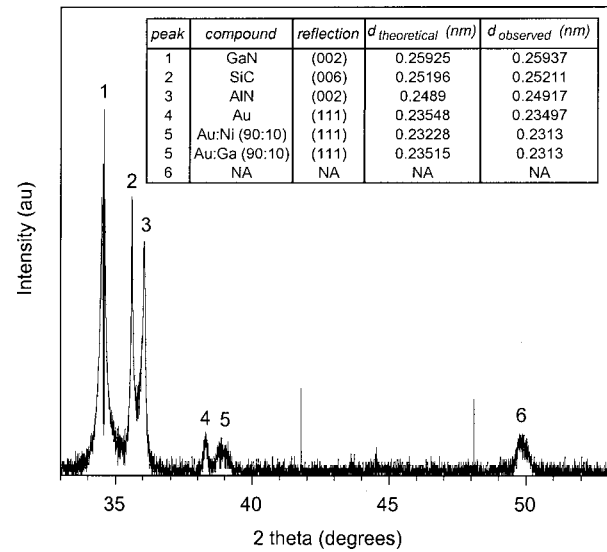


FIG. 9. X-ray diffraction (XRD) ω - 2θ plots for Ni/Au contacts on as-loaded *p*-type GaN surfaces following all thermal processing. The spectrum was acquired using Cu *K* α ($\lambda = 0.1542$ nm) radiation.

sition. The variation in the barrier height and the subsequent effects on ρ_c at each of the metal–semiconductor interfaces in the contact set would explain the excessive uncertainty in the as-deposited value of ρ_c for contact structures on the CVC surface. These effects may also be responsible for the nonlinear increase in total resistance with contact spacing for contact structures on as-loaded surfaces, which in turn precluded measurement of ρ_c .

Although there is a large uncertainty in the as-deposited value of the specific contact resistance for contacts on CVC surfaces, the data presented in Fig. 4 show significantly better ohmic behavior compared to identical contact structures on the as-loaded surface. It is important to note that even the least linear contact structures measured on the CVC surface

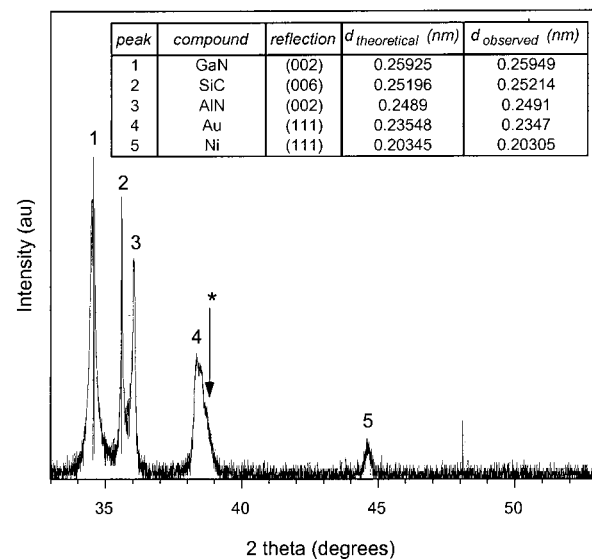


FIG. 10. X-ray diffraction (XRD) ω - 2θ plots for Ni/Au contacts on a CVC *p*-type GaN surface following all thermal processing. The spectrum was acquired using Cu *K* α ($\lambda = 0.1542$ nm) radiation.

exhibited less rectification over a finite voltage range compared to the most linear contacts measured on as-loaded surfaces in the as-deposited condition.

The significant improvement in the ohmic behavior of the as-loaded contacts following the postmetallization anneal is attributed to a dispersal of the native contamination at the semiconductor surface, which is consistent with previous reports in the literature.³² The removal of the contamination at the interface is accompanied by the formation of interfacial reaction products, as evidenced by the XRD spectrum in Fig. 9. The single broad peak identified as No. 5 in Fig. 9 is consistent with the formation of Au:Ga (90:10) and Au:Ni (90:10) solid solutions. Although the peaks for these two compounds could not be separated from the spectrum, the published value for the lattice parameter of Au:Ga (90:10) (Ref. 52) and those derived for Au:Ni (90:10), assuming Vegard's law, results in $d_{(111)}$ values for Au:Ga (90:10) and Au:Ni (90:10) of 0.2352 and 0.2323 nm, respectively. The theoretical values for the d spacing lie slightly above the calculated spacing for the center of peak 5. This may be attributed to Ga and/or Ni levels greater than 10% and/or tensile stress in the (111) plane due to the large mismatches in lattice parameter and coefficient of thermal expansion with the underlying GaN. The formation of Au:Ga solid solution is proposed to occur via the diffusion of Au through grain boundaries in the Ni whereupon it reacts with Ga at the interface.⁹

The aforementioned results are in stark contrast to the results observed in the behavior of the contacts deposited on the CVC surface. There was no change in the electrical properties of the contact structures on CVC surfaces following the postmetallization anneal, as indicated by the absence of any quantitative change in the electrical properties listed in Table III. This is consistent with the small variation in the I - V curves shown in Fig. 6 as well as the absence of any features in the XRD 2θ scan which would indicate substantial formation of interfacial reaction products. The shoulder observed on the Au (111) reflection shown in Fig. 10 may be due to the limited formation of Au-Ga, Au-Ni, or Au-Ga-Ni solid solutions. Note that the solubility limits of both Ni and Ga in Au at 450 °C have been reported⁵³ to be ~10%. However, the limited reactions that may occur at the interface do not appear to significantly change the electrical properties. The absence of any significant reactions at the metal-semiconductor interface is consistent with previous reports⁴⁵ of thermally stable contacts on clean semiconductor surfaces wherein the interface remained abrupt and unreacted upon annealing.

Due to the widespread disagreement regarding the temperature at which unique interfacial reaction products form, each possible Au-Ga phase⁵⁴ as well as previously reported Ni-Ga phases^{25,42} were systematically considered and eliminated prior to attributing peak 5 to the Au:Ga (90:10) and Au:Ni (90:10) (111) reflections. However, a Au-Ni-Ga solid solution could not be effectively ruled out.

The formation of a Au:Ga solid solution would extract Ga from the near surface region leaving behind Ga vacancies which could act as acceptors.⁵⁵ This would effectively increase the doping level in the near surface region and subse-

quently reduce the specific contact resistance at the interface. Alternatively, reactions at the metal-semiconductor interface may lead to interfacial roughening and/or metal protrusions into the p -GaN, which would result in field enhancement and a subsequent increase in the current passed through the interface.⁵⁶ In light of the fact that N vacancies are the thermodynamically favored defect in p -type GaN,⁵⁵ it is unlikely that a sufficient number of Ga vacancies would be generated in the near surface region and, therefore, the latter scenario is more probable. Within the calculated experimental error there was no difference in the specific contact resistance between the annealed contact structures on the CVC and the as-loaded surfaces. However, the results shown in Fig. 7 indicate that the magnitude of the current passed for annealed contacts on the as-loaded surface is greater at all voltages compared to identical contacts on CVC surfaces. The large uncertainty in the specific contact resistance due to material variation effectively eliminates the qualitative differences observed in the I - V data. The nature of this variation has been discussed in a previous section.

There are two possible scenarios that would explain the absence of the Ni (111) reflection in Fig. 9. The first is that the Ni overlayer was initially deposited on the contaminated GaN surface with no preferred orientation. However, previous reports of epitaxially deposited Ni on contaminated GaN surfaces^{13,36,41} effectively rule out this possibility. The second, more probable scenario is that the Ni was consumed by the overlying Au capping layer to form a Au:Ni solid solution as evidenced by peak 5 in Fig. 9. Regardless of whether the observed differences occurred in the as-deposited or annealed contact structures, it is important to note that there are significant structural differences between contact structures deposited on the CVC and the as-loaded surfaces. These findings are consistent with previous reports in other Group III-V systems.⁴⁵

V. SUMMARY

A NH_3 -based CVC process was used to obtain an ordered p -type GaN surface with no detectable C and a significantly reduced O concentration. As-deposited contact structures on CVC surfaces exhibited less rectification in the low voltage region (<2 V) compared to identical contact structures on the as-loaded surface. The improved ohmic behavior is attributed to the removal of native surface contamination prior to metal deposition and a subsequent reduction in the Schottky barrier height. Following a postmetallization anneal the values of ρ_c , ρ_s , and L_T for contacts on CVC surfaces remained unchanged and there was no substantial formation of interfacial reaction products. There was significant improvement in the ohmic behavior of the as-loaded contact following the postmetallization anneal. This is attributed to the dispersal of the native surface contamination, the formation of Au:Ga and Au:Ni solid solutions, and the subsequent roughening of the metal-semiconductor interface. The marked difference in the microstructure of the contact interface for contact structures on CVC and as-loaded surfaces is attributed to the effects of the native contamination on the thermal stability of the metal-semiconductor interface. Val-

ues of ρ_c for contacts on both as-loaded and CVC surfaces following a postmetallization anneal as well as during repeated thermal cycling to 140 °C were equivalent to within the calculated experimental error.

ACKNOWLEDGMENTS

This work was supported by the DoD Multidisciplinary University Research Initiative (MURI) program administered by the Office of Naval Research under Contract No. N00014-98-1-0654 (John Zolper, Monitor). The authors also acknowledge Cree, Inc. for the SiC substrates. R. F. D. was partially supported by the Kobe Steel, Ltd. Professorship. The authors would like to thank Dr. Raoul Schlessler, Dr. Scott Wolter, and Dr. Sven Einfeldt for helpful discussions. The authors also express their appreciation to D. Keough for performing the Hall measurements.

- ¹S. Nakamura, M. Senoh, N. Iwasa, and S. Nagahama, *Jpn. J. Appl. Phys.*, Part 2 **34**, L797 (1995).
- ²S. Yoshida and J. Suzuki, *Jpn. J. Appl. Phys.*, Part 2 **38**, L851 (1999).
- ³B. S. Shelton, D. J. H. Lambert, J. J. Huang, M. M. Wong, U. Chowdhury, T. G. Zhu, H. K. Kwon, Z. Liliental-Weber, M. Benarama, M. Feng, and R. S. Dupuis, *IEEE Trans. Electron Devices* **48**, 490 (2001).
- ⁴L. Zhang, L. F. Lester, A. G. Baca, R. J. Shul, P. C. Chang, C. G. Willison, U. K. Mishra, S. P. DenBaars, and J. C. Zolper, *IEEE Trans. Electron Devices* **47**, 507 (2000).
- ⁵N. Stath, V. Harle, and J. Wagner, *Mater. Sci. Eng.*, B **80**, 224 (2001).
- ⁶A. K. Fung, J. E. Borton, M. I. Nathan, J. M. Van Hove, R. Hickman II, P. Chow, and A. M. Wowchak, *J. Electron. Mater.* **28**, 572 (1999).
- ⁷J. M. DeLucca, H. S. Venugopalan, S. E. Mohney, and R. F. Karlicek, Jr., *Appl. Phys. Lett.* **73**, 3402 (1998).
- ⁸T. W. Kang, C. S. Chi, S. H. Park, and T. W. Kim, *Jpn. J. Appl. Phys.*, Part 1 **39**, 1062 (2000).
- ⁹J. K. Sheu, Y. K. Su, G. C. Chi, P. L. Koh, M. J. Jou, C. M. Chang, C. C. Liu, and W. C. Hung, *Appl. Phys. Lett.* **74**, 2340 (1999).
- ¹⁰L.-C. Chen, F. R. Chen, J.-J. Kai, L. Chang, J.-K. Ho, C.-S. Jong, C. C. Chiu, C.-N. Huang, C.-Y. Chen, and K.-K. Shih, *J. Appl. Phys.* **86**, 3826 (1999).
- ¹¹T. Kim, M. C. Yoo, and T. Kim, *Mater. Res. Soc. Symp. Proc.* **449**, 1061 (1997).
- ¹²J. K. Kim, J. L. Lee, J. W. Lee, Y. J. Park, and T. Kim, *J. Vac. Sci. Technol. B* **17**, 2675 (1999).
- ¹³J. K. Kim, J. H. Je, J.-L. Lee, Y. J. Park, and B.-T. Lee, *J. Electrochem. Soc.* **147**, 4645 (2000).
- ¹⁴D.-W. Kim, J. C. Bae, W. J. Kim, H. K. Baik, J.-M. Myoung, and S.-M. Lee, *J. Electron. Mater.* **30**, 183 (2001).
- ¹⁵J. K. Kim, J.-L. Lee, J. W. Lee, Y. J. Park, and T. Kim, *Electron. Lett.* **35**, 1676 (1999).
- ¹⁶J. K. Kim, J. H. Je, J. W. Lee, Y. J. Park, T. Kim, I.-O. Jung, B.-T. Lee, and J.-L. Lee, *J. Electron. Mater.* **30**, L8 (2000).
- ¹⁷J. K. Kim, K. J. Kim, B. Kim, J. N. Kim, J. S. Kwak, Y. J. Park, and J.-L. Lee, *J. Electron. Mater.* **30**, 129 (2001).
- ¹⁸J. K. Kim, J.-L. Lee, J. W. Lee, H. E. Shin, Y. J. Park, and T. Kim, *Appl. Phys. Lett.* **73**, 2953 (1998).
- ¹⁹J. K. Kim, C. C. Kim, T. S. Cho, J. H. Je, J. S. Kwak, Y. J. Park, and J.-L. Lee, *J. Electron. Mater.* **30**, 170 (2001).
- ²⁰M.-R. Park, W. A. Anderson, and S.-J. Park, *MRS Internet J. Nitride Semicond. Res.* **5S1**, W11.77 (2000).
- ²¹J.-L. Lee, J. K. Kim, J. W. Lee, Y. J. Park, and T. Kim, *Solid-State Electron.* **43**, 435 (1999).
- ²²T. Mori, T. Kozawa, T. Ohwaki, Y. Taga, S. Nagai, S. Yamasaki, S. Asami, N. Shibata, and M. Koike, *Appl. Phys. Lett.* **69**, 3537 (1996).
- ²³J.-S. Jang, S.-J. Park, and T.-Y. Seong, *J. Appl. Phys.* **88**, 5490 (2000).
- ²⁴J.-S. Jang, S.-J. Park, and T.-Y. Seong, *J. Vac. Sci. Technol. B* **17**, 2667 (1999).
- ²⁵R. Wenzel, G. G. Fischer, and R. Schmid-Fetzer, *Mater. Sci. Semicond. Process.* **4**, 357 (2001).
- ²⁶I. P. Smorchkova, E. Haus, B. Heying, P. Kozodoy, P. Fini, J. P. Ibbetson, S. Keller, S. P. DenBaars, J. S. Speck, and U. K. Mishra, *Appl. Phys. Lett.* **76**, 718 (2000).
- ²⁷H. Amano, M. Kito, K. Hiramatsu, and I. Akasaki, *Jpn. J. Appl. Phys.*, Part 2 **28**, L2112 (1989).
- ²⁸P. Kozody, S. Keller, S. P. DenBaars, and U. K. Mishra, *J. Cryst. Growth* **195**, 265 (1998).
- ²⁹S. Strite and H. Morkoc, *J. Vac. Sci. Technol. B* **10**, 1237 (1992).
- ³⁰T. Usagawa, M. Kobayashi, T. Mishima, P. D. Rabinzohn, A. Ihara, M. Kawata, T. Yamada, E. Tokumitsu, M. Konagai, and K. Takahashi, *J. Appl. Phys.* **69**, 8227 (1991).
- ³¹S. W. King, J. P. Barnak, M. D. Bremser, K. M. Tracy, C. Ronning, R. F. Davis, and R. J. Nemanich, *J. Appl. Phys.* **84**, 5248 (1998).
- ³²H. Ishikawa, S. Kobayashi, Y. Koide, S. Yamasaki, S. Nagai, J. Umezaki, M. Koide, and M. Murakami, *J. Appl. Phys.* **81**, 1315 (1997).
- ³³P. J. Hartlieb, A. Roskowski, R. F. Davis, W. Platow, and R. J. Nemanich, *J. Appl. Phys.* **91**, 732 (2002).
- ³⁴A. Lahav, M. Eizenberg, and Y. Komem, *J. Appl. Phys.* **60**, 991 (1986).
- ³⁵T. Sands, V. G. Keramidis, A. J. Yu, K.-M. Yu, R. Gronsky, and J. Washburn, *J. Mater. Res.* **2**, 262 (1987).
- ³⁶Q. Z. Liu, S. S. Lau, N. R. Perkins, and T. F. Kuech, *Appl. Phys. Lett.* **69**, 1722 (1996).
- ³⁷I. Waki, H. Fujioka, K. Ono, M. Oshima, H. Miki, and A. Fukuzawa, *Jpn. J. Appl. Phys.*, Part 1 **39**, 4451 (2000).
- ³⁸J. Sun, K. A. Rickert, J. M. Redwing, A. B. Ellis, F. J. Himpsel, and T. F. Kuech, *Appl. Phys. Lett.* **76**, 415 (2000).
- ³⁹C. I. Wu and A. Kahn, *J. Vac. Sci. Technol. B* **16**, 2218 (1998).
- ⁴⁰R. Wenzel, G. G. Fischer, and R. Schmid-Fetzer, *Mater. Sci. Semicond. Process.* **4**, 367 (2001).
- ⁴¹Y. Koide, T. Maeda, T. Kawakami, S. Fujita, T. Uemura, N. Shibata, and M. Murakami, *J. Electron. Mater.* **28**, 341 (1999).
- ⁴²J. K. Sheu, Y. K. Su, G. C. Chi, W. C. Chen, C. Y. Chen, C. N. Huang, J. M. Hong, Y. C. Yu, C. W. Wang, and E. K. Lin, *J. Appl. Phys.* **83**, 3172 (1998).
- ⁴³C. C. Kim, J. K. Kim, J.-L. Lee, J. H. Je, M.-S. Yi, D. Y. Noh, Y. Hwu, and P. Ruterana, *MRS Internet J. Nitride Semicond. Res.* **6**, 4 (2001).
- ⁴⁴C. C. Kim, J. K. Kim, J.-L. Lee, J. H. Je, M.-S. Yi, D. Y. Noh, Y. Hwu, and P. Ruterana, *Appl. Phys. Lett.* **78**, 3773 (2001).
- ⁴⁵Z. Liliental-Weber, E. R. Weber, and N. Newman, in *Contacts to Semiconductors*, edited by L. J. Brillson (Noyes, Park Ridge, NJ, 1993), Chap. 6.
- ⁴⁶A. R. Smith, R. M. Feenstra, D. W. Greve, M.-S. Shin, M. Skowronski, J. Neugebauer, and J. E. Northrup, *Appl. Phys. Lett.* **72**, 2114 (1998).
- ⁴⁷W. Gotz, N. M. Johnson, J. Walker, D. P. Bour, H. Amano, and I. Akasaki, *Appl. Phys. Lett.* **67**, 2666 (1995).
- ⁴⁸D. K. Schroder, *Semiconductor Material and Device Characterization* (Wiley, New York, 1998), p. 156.
- ⁴⁹S. D. Wolter, J. M. Delucca, S. E. Mohney, R. S. Kern, and C. P. Kuo, *Thin Solid Films* **371**, 153 (2000).
- ⁵⁰D. Briggs and M. P. Seah, *Practical Surface Analysis Volume 1* (Wiley, West Sussex, 1983), p. 543.
- ⁵¹P. Kozodoy, S. P. DenBaars, and U. K. Mishra, *J. Appl. Phys.* **87**, 770 (2000).
- ⁵²C. J. Cooke, and W. Hume-Rothery, *J. Less-Common Met.* **10**, 42 (1966).
- ⁵³T. B. Masalski and H. Okamoto, in *Phase Diagrams of Binary Gold Alloys*, edited by H. Okamoto and T. B. Masalski (ASM, Materials Park, 1987), pp. 111, 193.
- ⁵⁴*Pearson's Handbook of Crystallographic Data for Intermetallic Phases*, edited by P. Villars and L. D. Calvert (ASM, Materials Park, 1991), p. 1285.
- ⁵⁵J. Neugebauer and C. G. Van de Walle, *Mater. Res. Soc. Symp. Proc.* **395**, 645 (1996).
- ⁵⁶N. Braslau, *J. Vac. Sci. Technol.* **19**, 803 (1981).